Electronic Supplementary Information (ESI)

Stability of europium(II) in nitrate aqueous media

Michiel Van de Voorde, Bart Geboes, Tom Vander Hoogerstraete, Karen Van Hecke,

Thomas Cardinaels, and Koen Binnemans*

1 Cyclic voltammetry experiments

1.1 Europium-free solutions

Cyclic voltammetry experiments of the blank solutions containing different nitrate salt-based supporting electrolytes were performed. The resulting CVs show that the investigated blank media are all redox stable in the potential window studied. No additional reduction or oxidation peaks arise from any of the blank solutions, proving their electrochemical inertness. Therefore, reduction and oxidation signals acquired in solutions containing europium can be assigned to Eu^{3+}/Eu^{2+} redox couple.

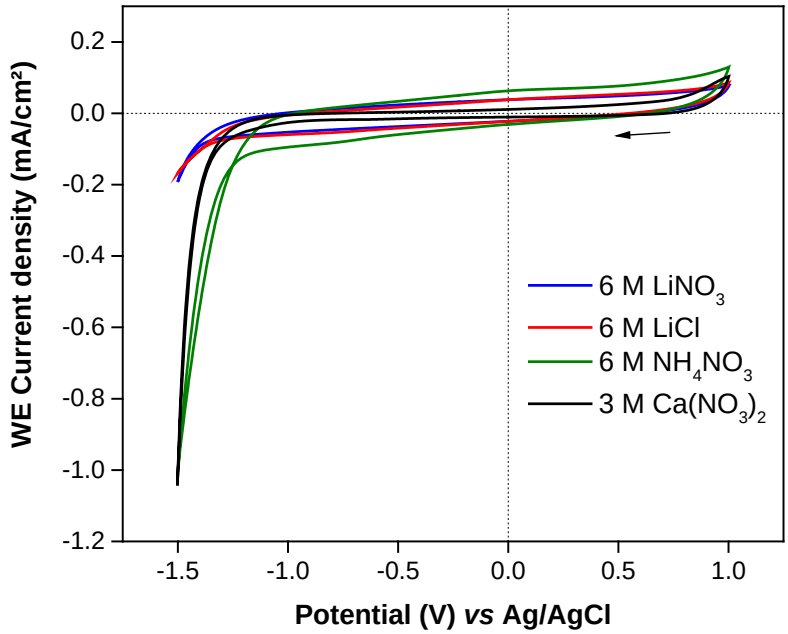

Figure S1: Cyclic voltammograms (second cycle) of blank solutions containing 6 mol L^{-1} nitrate or chloride anions, making use of different counter ions (Li^+, Ca^{2+}, NH_4^+). WE: glassy carbon, RE: Ag/Ag^+ in 0.1 mol L^{-1} KCl, CE: Pt wire, scan rate: 100 mV s^{-1}.

A cyclic voltammetry measurement was performed on a solution containing a lanthanide ion other than europium, i.e. samarium, which is electrochemically inert in the conditions applied. As can be seen in Figure S2, no reduction or oxidation peaks are present in the cyclic

voltammogram, denoting the absence of any redox active species in solution. This way, it was demonstrated that the reduction and oxidation peaks occurring in the cyclic voltammetry measurements on europium-containing solutions originate solely from the Eu^{3+}/Eu^{2+} redox couple.

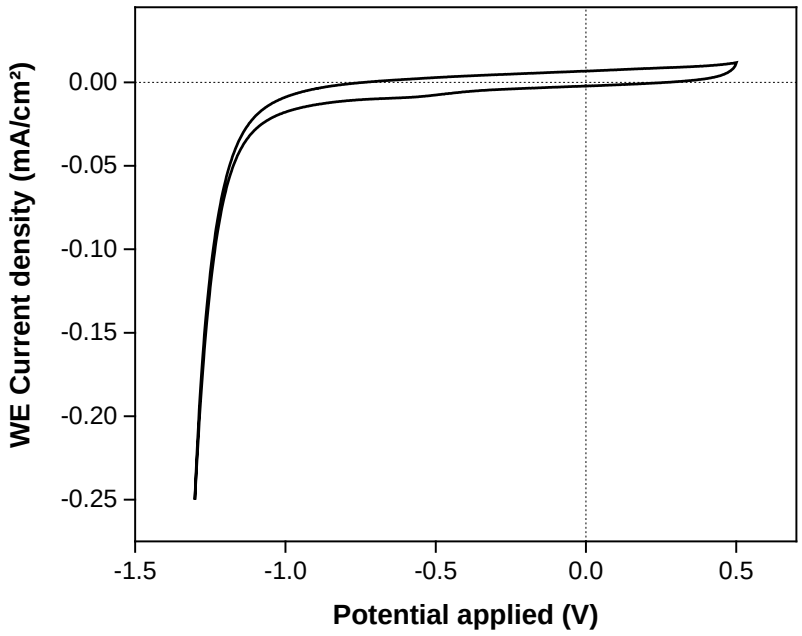

Figure S2: Cyclic voltammograms (second cycle) of a solution containing 10 mmol L^{-1} Sm and 3 mol L^{-1} $Ca(NO_3)_2$. WE: glassy carbon, RE: Ag/Ag^+ in 3 mol L^{-1} KCl, CE: Pt wire, scan rate: 100 mV s^{-1}.

1.2 Relation of peak current density and viscosity

A change of the supporting electrolyte concentration in a solution also leads to changes in the physical properties of the solution. In particular, *viscosity η* and *density ρ* of the solution are affected. In electrochemical experiments, viscosity of the solution has a major influence on the behavior of the electrochemical cell. The mass transfer and the *diffusion coefficient D* are inversely proportional to the viscosity of the solution *via* the Stokes-Einstein equation (Eq. S1).

$$D = \frac{\mathrm{k_B}T}{6\pi\eta r} \quad \text{(S1)}$$

where k_B is the Boltzmann's constant, T the absolute temperature, η the dynamic viscosity and r the radius of particle. The *peak current* i_P and *peak current density* j_P are proportional to the square root of the diffusion coefficient according to the Randles-Sevcik equation (Eq. S2, at 25 °C). A change in current density upon changing salt concentration, as was observed in the cyclic voltammetry experiments in this study, can be (partially) explained by a change in viscosity. For this reason, it is important to measure the viscosity of the solutions used in electrochemical experiments.

$$i_P = (2.69 \times 10^5) n^{3/2} A {D_O}^{1/2} C_O^* v^{1/2} \quad \text{(S2)}$$

where i_P is the peak current in amperes, n the number of electrons transferred in the redox event, A the surface area in cm² of the work electrode, D_O the diffusion coefficient of the redox sensitive species in cm² s^{-1}, C_O^* the bulk concentration of the redox sensitive species in mol cm^{-3} and υ the linear potential scan rate in V s^{-1}.

The viscosities of the solutions containing 10 mmol L^{-1} europium and different concentrations of $Ca(NO_3)_2$ and $CaCl_2$ were measured *via* the rolling ball principle using an Anton Paar Lovis 2000 M/ME viscometer. A capillary with inner diameter of 1.59 mm was used. The average viscosity was determined on seven measurements. For completeness, density of the saline solutions was measured simultaneously using an Anton Paar DMA 4500 M. Results of these measurements are listed in Table S1.

Table S1: Dynamic and kinematic viscosity (with variation coefficient) and density of the different saline solutions used in electrochemical experiments. All solutions contained 10 mmol L^{-1} europium and were measured at 25 °C.

Salt concentration	Dynamic viscosity (mPa s)	Kinematic viscosity ($mm^2\ s^{-1}$)	Density ($g\ cm^{-3}$)
0 mol L^{-1} $Ca(NO_3)_2$	0.846 ± 0.001	0.842 ± 0.001	1.00
0.5 mol L^{-1} $Ca(NO_3)_2$	0.941 ± 0.003	0.889 ± 0.003	1.06
1.5 mol L^{-1} $Ca(NO_3)_2$	1.272 ± 0.002	1.086 ± 0.001	1.17
3 mol L^{-1} $Ca(NO_3)_2$	2.482 ± 0.002	1.866 ± 0.001	1.33
4.5 mol L^{-1} $Ca(NO_3)_2$	5.866 ± 0.005	3.985 ± 0.004	1.47
0 mol L^{-1} $CaCl_2$	0.844 ± 0.001	0.844 ± 0.001	1.00
0.5 mol L^{-1} $CaCl_2$	0.935 ± 0.001	0.896 ± 0.001	1.04
1.5 mol L^{-1} $CaCl_2$	1.258 ± 0.001	1.111 ± 0.001	1.13
3 mol L^{-1} $CaCl_2$	2.383 ± 0.001	1.890 ± 0.001	1.26
4.5 mol L^{-1} $CaCl_2$	5.988 ± 0.002	4.342 ± 0.002	1.38

The peak current density as a function of the viscosity is plotted in Figure S3 (similar to Figure 5 in the main manuscript). These data were analyzed by Origin 2016 software by fitting the curves using a $f(x) = a \cdot x^b$ function model (allometric). Outcome of the function parameters *a* and *b* and the accompanying coefficient of determination (R^2, adjusted) after curve analysis

can be found in Table S2. This curve analysis proves that the peak current density is indeed inversely proportional to the square root of the viscosity, as was discussed before.

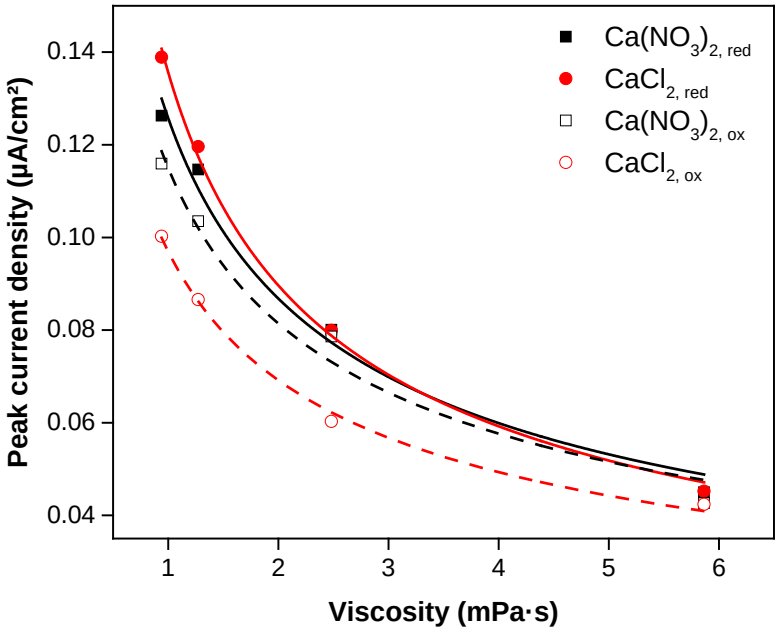

Figure S3: Curve fitting of the peak current density as a function of the viscosity (Figure 5 in main manuscript) via the function model $f(x) = a \cdot x^b$. Scan rate: 50 mV s^{-1}.

Table S2: Outcome of the curve parameters a and b for a function $f(x) = a \cdot x^b$ after curve analysis of the peak current density as a function of the viscosity.

Medium	**a**	**b**	**R^2**
$Ca(NO_3)_{2,\ red}$	1.26E-4 ± 3.89E-6	-0.54 ± 0.052	0.98057
$CaCl_{2,\ red}$	1.36E-4 ± 1.93E-6	-0.60 ± 0.025	0.99633
$Ca(NO_3)_{2,\ ox}$	1.15E-4 ± 4.30E-6	-0.50 ± 0.060	0.96924
$CaCl_{2,\ ox}$	9.70E-5 ± 1.34E-6	-0.49 ± 0.022	0.99539

1.3 Peak potential and peak separation potential

The peak potential for reduction ($E_{P,c}$) and oxidation ($E_{P,a}$) of europium (10 mmol L^{-1}) and the resulting peak separation potential (ΔE_P) in various nitrate and chloride aqueous solutions are listed in Table S3 and Table S4, respectively.

Table S3: Peak potentials and peak separation potentials of cathodic and anodic sweep for 10 mmol L^{-1} europium in various nitrate aqueous media (second cycle). Scan rate 0.05 V s^{-1}.

$[Ca(NO_3)_2]$ (mol L^{-1})	**$E_{P,c}$ (V)**	**$E_{P,a}$ (V)**	**ΔE_P (V)**
0.5	-0.647	-0.563	0.084
1.5	-0.619	-0.524	0.095
3	-0.579	-0.468	0.111
4.5	-0.531	-0.409	0.122

Table S4: Peak potentials and peak separation potentials of cathodic and anodic sweep for 10 mmol L^{-1} europium in various chloride aqueous media (second cycle). Scan rate: 0.05 V s^{-1}.

$[CaCl_2]$ (mol L^{-1})	**$E_{P,c}$ (V)**	**$E_{P,a}$ (V)**	**ΔE_P (V)**
0.5	-0.674	-0.504	0.170
1.5	-0.647	-0.472	0.175
3	-0.595	-0.389	0.206
4.5	-0.551	-0.230	0.321

1.4 Relation of peak current density and europium concentration

Cyclic voltammograms of 3 mol L^{-1} $Ca(NO_3)_2$ solutions containing different europium concentrations, *i.e*. 1, 5, 10, 50 and 100 mmol L^{-1}, were recorded (Figure S4). The cathodic peak current density j_P of each reduction peak was plotted as a function of the europium concentration in Figure S5. This plot clearly shows that the absolute value of the peak current density is linearly proportional with the europium concentration in solution. This result follows the Randles-Sevcik equation (Eq. S2), where concentration is proportional to (peak) current density. After all, the Faradaic current is a direct measure of the electrochemical reactions taking place at the electrode surface. Consequently, the resulting peaks in the cyclic voltammograms can be assigned to the reduction and oxidation of europium.

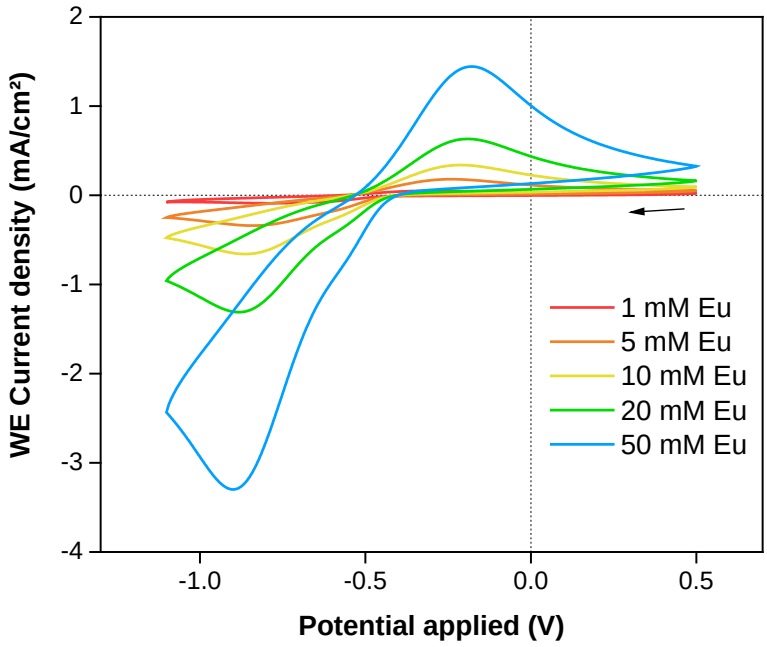

Figure S4: Cyclic voltammograms (second cycle) of solutions containing different europium concentrations and 3 mol L^{-1} $Ca(NO_3)_2$. WE: glassy carbon, RE: Ag/Ag^+ in 3 mol L^{-1} KCl, CE: Pt wire, scan rate: 100 mV s^{-1}.

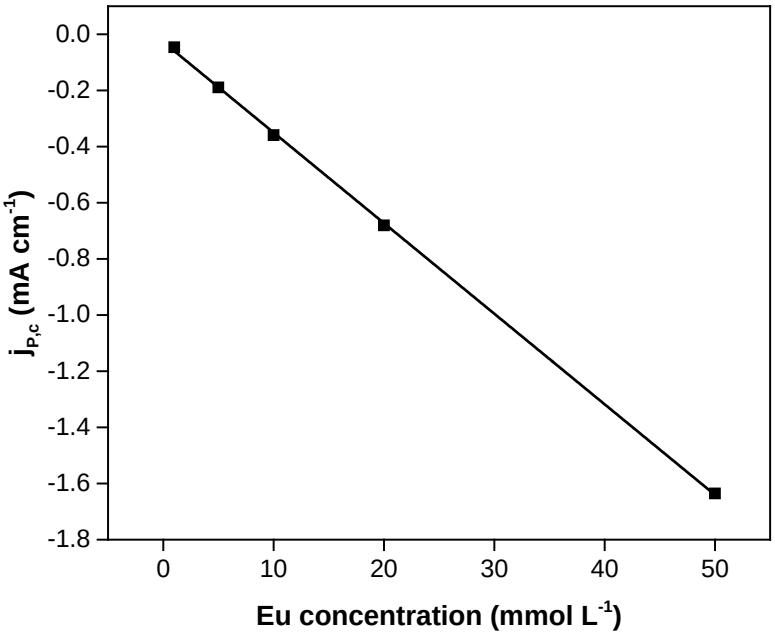

Figure S5: Cathodic peak current densities as a function of the europium concentration in 3 mol L^{-1} $Ca(NO_3)_2$ solutions (R^2: 0.99979).

1.5 Relation of peak current density and scan rate

Cyclic voltammetry measurements were conducted on solutions containing 10 mmol L^{-1} europium and 3 mol L^{-1} $Ca(NO_3)_2$ using different scan rates, *i.e*. 10, 20, 50, 100, 200, 300, 500 and 1000 mV s^{-1} (Figure S6). According to the Randles-Sevcik equation (Eq. S2), the (peak) current density is proportional to the square root of the scan rate in a reversible system. The resulting plot of the peak current density as a function of the square root of the scan rate does not result in a perfect linear correlation (Figure S7). The shift in the peak potential as a function of scan rate indicates that there is no contribution of surface-adsorbed species (Figure S8), so that the deviation from linearity indicates a quasi-reversible system. The quasi-reversible nature of the Eu^{3+}/Eu^{2+} redox system is confirmed by the increase in peak separation potential as a function of the scan rate.

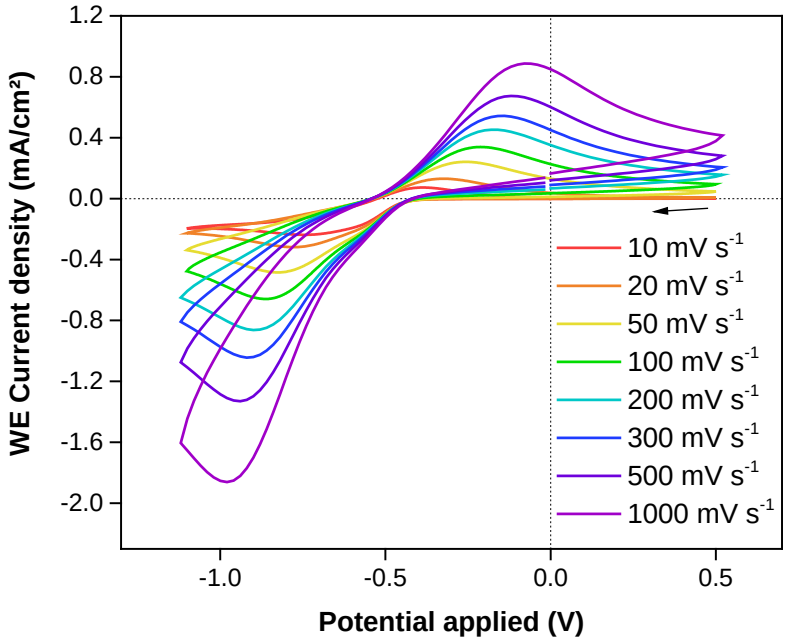

Figure S6: Cyclic voltammograms (second cycle) of solutions containing 10 mmol L^{-1} Eu and 3 mol L^{-1} $Ca(NO_3)_2$ using different scan rates. WE: glassy carbon, RE: Ag/Ag^+ in 3 mol L^{-1} KCl, CE: Pt wire.

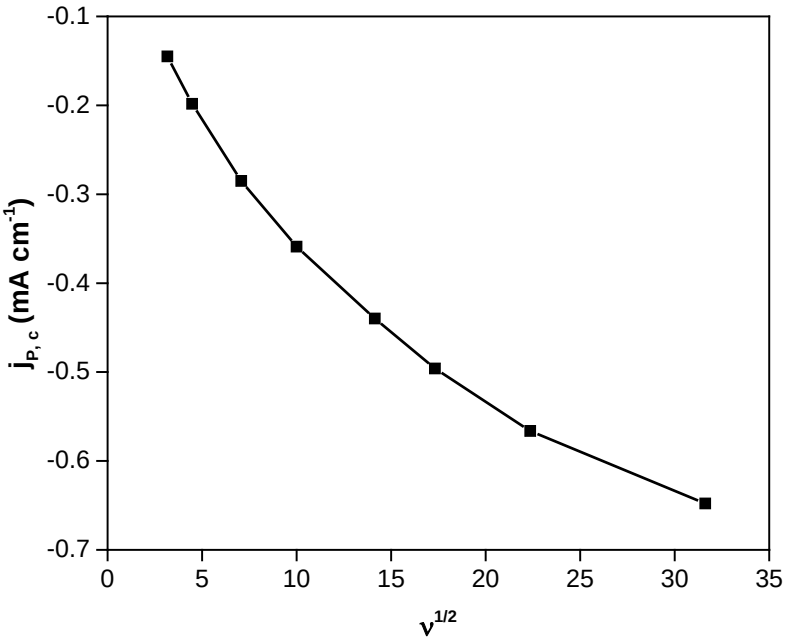

Figure S7: Cathodic peak current densities as a function of the square root of the scan rate using a solution containing 10 mmol L^{-1} Eu and 3 mol L^{-1} $Ca(NO_3)_2$.

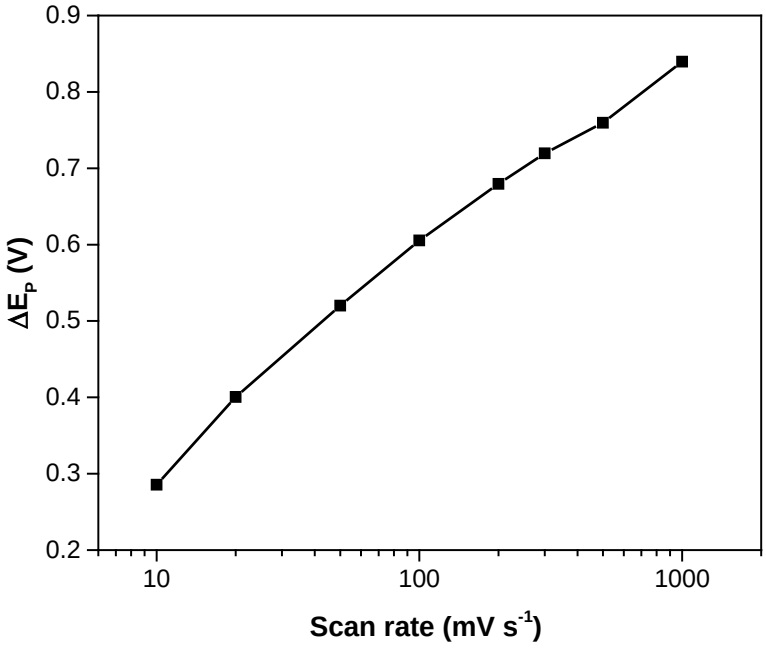

Figure S8: Peak separation potentials as a function of the scan rate (logarithmic scale) using a solution containing 10 mmol L^{-1} Eu and 3 mol L^{-1} $Ca(NO_3)_2$.

2 UV-VIS absorption measurements

Solutions containing different Eu^{2+} concentrations changed color from (pale) yellow to orange with increasing europium concentration (see Figure 1 main manuscript). For this reason, UV-VIS absorption measurements were performed on solutions containing different Eu^{2+} concentrations, *i.e*. 3.29, 6.58, 32.9 and 65.8 mmol L^{-1} (Figure S9 and Figure S10). From these spectra, it is evident that the broad absorption bands slightly shift towards longer wavelengths with increasing Eu^{2+} concentration, *i.e*. a red shift or bathochromic effect. This shift is the origin of the color change of the solution as a function of the europium concentration.

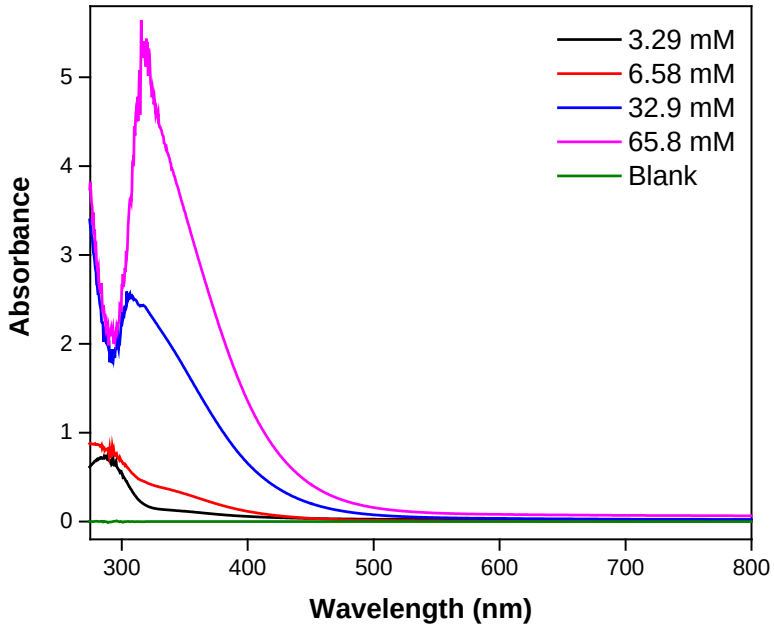

Figure S9: UV-VIS absorption spectra in terms of absorbance of solutions containing different Eu^{2+} concentrations in 3 mol L^{-1} $Ca(NO_3)_2$. Lamp changeover occurred at 350 nm. A path length of 1 mm, a resolution of 0.5 nm and a scan rate of 150 nm min^{-1} were used.

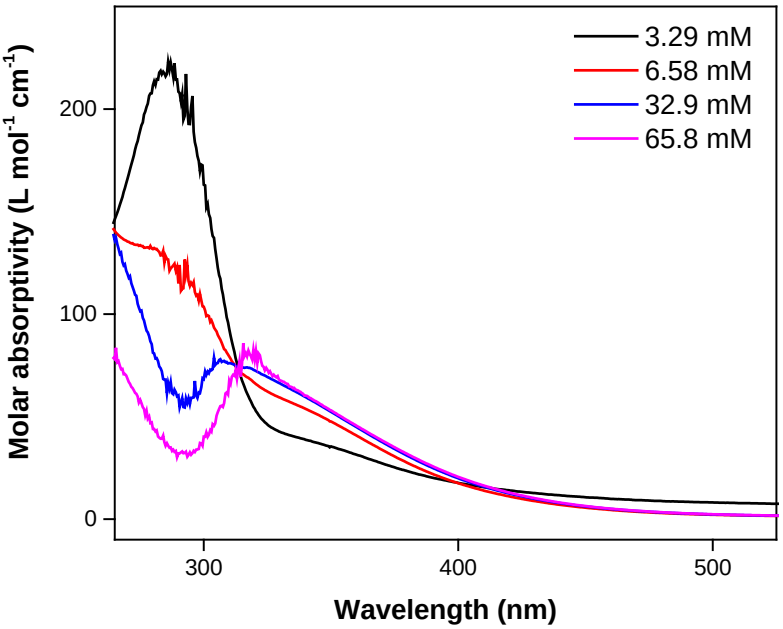

Figure S10: UV-VIS absorption spectra in terms of molar absorptivity of solutions containing different Eu^{2+} concentrations in 3 mol L^{-1} $Ca(NO_3)_2$. Lamp changeover occurred at 350 nm. A path length of 1 mm, a resolution of 0.5 nm and a scan rate of 150 nm min^{-1} were used.

UV-VIS absorption spectra of Eu^{3+} in 3 mol L^{-1} $Ca(NO_3)_2$ and $CaCl_2$ solutions were recorded for comparison with the Eu^{2+} UV-VIS spectra in these media. The resulting spectra are shown in Figure S11. Spectra were limited to 320 nm because of the strong absorption by nitrate ions at shorter wavelengths, and consequently the low reliability of the detector signal. The fine structure of Eu^{3+} with very low molar absorptivity is clearly present in both spectra, and are very comparable in both media. The most intense absorption band is located at 390-400 nm, and originates from the $^5L_6 \leftarrow {}^7F_0$ transition. A smaller peak at 400-410 nm, originating from the $^5L_6 \leftarrow {}^7F_1$ present as a shoulder of this intense absorption peak. The smaller absorption bands at 355-370 nm originate from the weak f-f transitions from the ground state $^7F_0$ and the first excited multiplet $^7F_1$ to the multiplet manifolds $^5D_0$, $^5D_1$ and $^5D_2$. More detailed information on the interpretation of Eu^{3+} spectra can be found in the comprehensive review by Binnemans.[1]

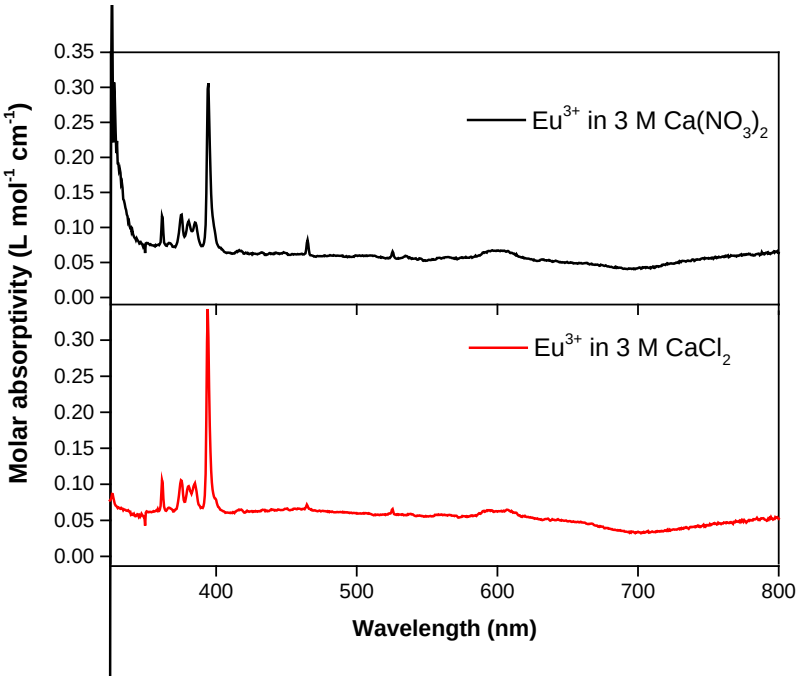

Figure S11: UV-VIS absorption spectra of Eu^{3+} (6.6 mmol L^{-1}) in aqueous nitrate and chloride media (3 mol L^{-1} CaX_2, with X NO_3^- or Cl^-). Blank solutions of the respective aqueous media were used for background correction. The lamp changeover occurred at 350 nm. A path length of 10 mm, a resolution of 0.5 nm and a scan rate of 150 nm min^{-1} were used.

3 Magnetic susceptibility measurements of europium in chloride aqueous media

With the exception of La^{3+} and Lu^{3+}, all Ln^{3+} ions contain unpaired electrons, and are therefore paramagnetic. In general, the magnetic properties of lanthanide ions are determined entirely by the ground state, as the excited states are well separated from the ground state owing to the spin–orbital coupling, making them thermally inaccessible. Therefore, the magnetic properties of Ln^{3+} ions are independent of the environment as they are only determined by the electron configuration of the free ion. However, for Eu^{3+} ([Xe] $4f^6$), the ground state ($^7F_0$) does not contribute to the magnetic moment despite its six unpaired electrons. The orbital angular momentum of Eu^{3+} cancels out the electron angular momentum, whereby Eu^{3+} is considered diamagnetic at 0 K. Nevertheless, the first excited state of Eu^{3+} ($^7F_1$) is thermally accessible at room temperature and contributes to the magnetic moment, resulting in overall moderate paramagnetic properties of Eu^{3+} at room temperature.[2] Because the magnetic properties of Eu^{3+} are predominantly determined by the occupation of the $^7F_1$ energy level, differences in Eu^{3+} coordination can affect the resulting effective magnetic moment since the energy difference between the ground state ($^7F_0$) and the first excited state ($^7F_1$) depends on the environment of Eu^{3+} at a given temperature. Contrarily, Eu^{2+} ([Xe] $4f^7$) is strongly paramagnetic (μ_B = 7.63 - 8.43) in its ground state ($^8S_{7/2}$, *i.e.* similar to Gd^{3+}) because of its seven unpaired electrons.[3]

The change in effective magnetic moment upon chemical and electrochemical reduction of Eu^{3+} in concentrated nitrate aqueous media (3 mol L^{-1} $Ca(NO_3)_2$) was compared to the chemical reduction of europium in concentrated chloride aqueous media (6 mol L^{-1} LiCl) by means of magnetic susceptibility measurements. The volume magnetic susceptibility as a

function of the reduction time is presented in Figure S12. The parameters of the exponential fit for these curves are presented in Table S2. Reduction of europium in aqueous chloride media appears to be slightly more efficient, reaching the plateau value already after 90 min. A plateau value in aqueous nitrate media, for both chemical and electrochemical reduction, was only reached after *ca*. 120 min. The difference in value for the volume magnetic susceptibility in both aqueous media can be attributed to the different solvent matrix, which contain different species with different effective magnetic moment (see main article), and a small variation in the total europium concentration in both samples. The magnetic susceptibility balance is highly sensitive to the composition of the samples.

Magnetic susceptibility measurements of a sample stored in a sealed sample tube after electrochemical reduction indicate the high stability of Eu^{2+} in nitrate media (Figure S13).

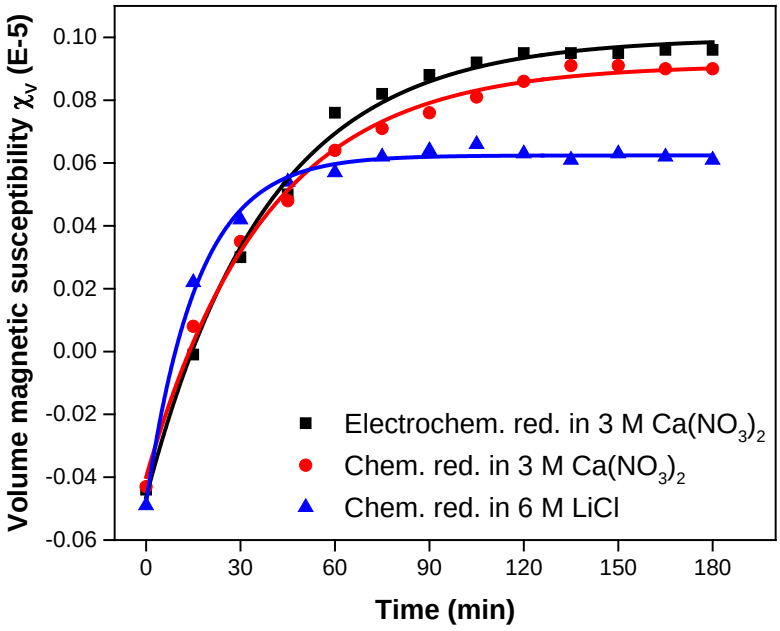

Figure S12: Comparison of the reducibility of europium in aqueous nitrate and chloride media via magnetic susceptibility measurements. Electrochemical (black, squares) and chemical (red, circles) reduction of 66 mmol L^{-1} Eu^{3+} in 3 mol L^{-1} $Ca(NO_3)_2$ aqueous solution are compared to the chemical reduction of 66 mmol L^{-1} Eu^{3+} in a 6 mol L^{-1} LiCl (blue, triangles) aqueous solution. A fresh aliquot was measured every 15 min for 3 h at room temperature.

Table S5: Outcome of the curve parameters A, y_0 and R_0 for the function model $f(x) = y_0 + A \cdot e^{R_0 \cdot x}$ for the curve analysis of the volume magnetic susceptibility as a function of the reduction time.

Medium	A	y_0	R_0
$Ca(NO_3)_{2,\ elect.\ red.}$	-0.146 ± 0.003	0.0998 ± 0.0018	-0.0261 ± 0.0014
$Ca(NO_3)_{2,\ chem.\ red.}$	-0.131 ± 0.003	0.0912 ± 0.0016	-0.0264 ± 0.0014
$LiCl_{chem.\ red.}$	0.950 ± 0.045	0.0624 ± 0.008	-0.0617 ± 0.0031

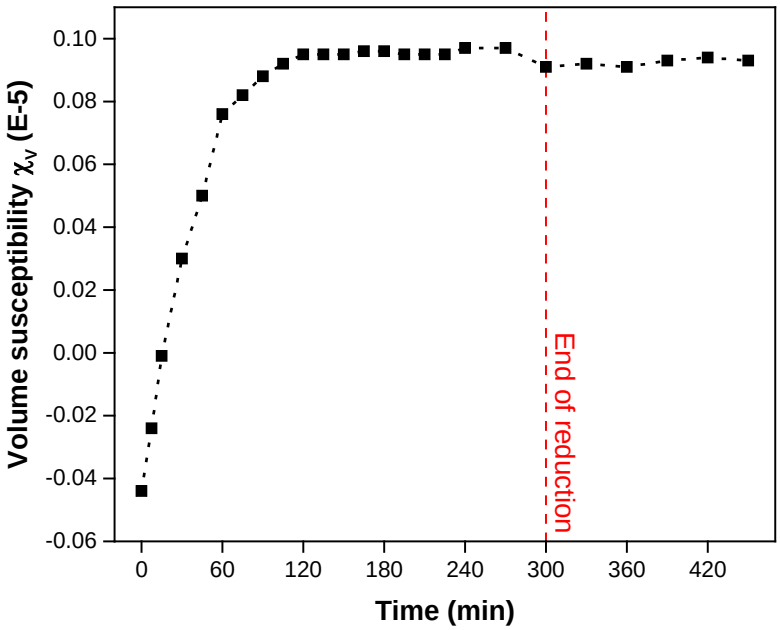

Figure S13: Magnetic susceptibility measurements of the electrochemical reduction of 66 mmol L^{-1} Eu^{3+} in a 3 mol L^{-1} $Ca(NO_3)_2$ aqueous solution. The reduction was stopped after 300 min, after which the sample was stored in a sealed sample tube and measured every 30 min for the next 150 min.

4 XAFS measurements

X-ray absorption near-edge structure (XANES) is a technique that is frequently being applied to investigate the relative amounts of Eu^{2+} and Eu^{3+} in chemical, physical and geological surveys. In XANES measurements, high-energy X-rays from a synchrotron source are being used to irradiate the sample. Absorption of these X-rays by an atom leads to the ejection of a core electron. The energy at which this electron is ejected, *i.e*. the edge, is specific for each element. The divalent and trivalent oxidation states of europium can be easily distinguished by making use of the L_{III} absorption edge around 6977 eV. The XANES spectra show distinct resonance peaks, *i.e*. white lines, for Eu^{2+} and Eu^{3+}. Both resonance peaks are separated by *ca*. 8 eV, at 6971.3 and 6979.3 eV, respectively. The resonance peaks originate from the electron transitions between $2p_{3/2}$ and 5*d* electronic states. Increased shielding of the nucleus by the additional 4f electron results in a slightly lower binding energy of the core electrons in Eu^{2+}. This is the main reason for the resonance peak for Eu^{2+} being observed at a slightly lower X-ray energy. In addition to the resonance peaks, the spectrum contains continuum steps at which the core electron is excited to a continuum of final states such as free electron states.[4] These transitions to the continuum occur at slightly higher energies than the $2p_{3/2} \rightarrow 5d$ transitions. The L adsorption edge or continuum step, at which a 2*p* electron is excited to different energy levels, has to be accounted for when deconvoluting the XANES spectra. However, the adsorption edge step is difficult to examine experimentally as it is usually obscured by other spectral features.[4] The line shape of the continuum step, *i.e*. the transition to unoccupied cluster orbitals in the metal, is represented by a single Lorentzian function, with a width determined principally by the 2*p* core hole lifetime.[5] Integration of this

function yields an arctangent function, which can be used for simulation of the continuum step. Such arctangent function was constructed for both Eu^{2+} and Eu^{3+}.

4.1 Arctangent background subtraction and peak deconvolution

After pre-edge background subtraction, the arctangent background was accounted for using Equation S3 as a function of the energy (in eV):

$$f(\mathrm{E}) = \frac{(\mathrm{Eu}^{2+})_{\mathrm{RF}}}{\pi}\left(\operatorname{atan}\left(\frac{\pi}{\mathrm{R}}\left(\mathrm{E} - \mathrm{E}_{\mathrm{Eu}^{2+},\mathrm{RP}}\right)\right) + \frac{\pi}{2}\right) + \frac{(\mathrm{Eu}^{3+})_{\mathrm{RF}}}{\pi}\left(\operatorname{atan}\left(\frac{\pi}{\mathrm{R}}\left(\mathrm{E} - \mathrm{E}_{\mathrm{Eu}^{3+},\mathrm{RP}}\right)\right) + \frac{\pi}{2}\right) \quad \text{(S3)}$$

With $(Eu^{2+})_{RF}$ and $(Eu^{3+})_{RF}$ the relative fractions of Eu^{2+} and Eu^{3+} in the sample, respectively; R the resolution of the arctangent function (a resolution of 5 was used); $\mathrm{E}_{\mathrm{Eu}^{2+},\mathrm{RP}}$ and $\mathrm{E}_{\mathrm{Eu}^{3+},\mathrm{RP}}$ the position of the resonance peaks for Eu^{2+} (6971.5 eV) and Eu^{3+} (6979.5 eV), respectively. Sum of the relative fractions of Eu^{2+} and Eu^{3+} (total height of the arctangent jump) is equal to 1 as the absorbance in the XANES spectra were normalized to 1. Examples of the arctangent background for a sample containing 100% Eu^{3+} (0 min of chemical reduction) and a sample containing *ca*. 82% Eu^{2+} and *ca*. 18% Eu^{3+} (90 min of chemical reduction) are presented in Figure S14 and Figure S15, respectively. An example of the resulting peak deconvolution using multiple peak analysis (via Origin 2016 software) by means of Pseudo-Voigt functions is shown in Figure S16. The parameters of the exponential fit for the curves of the relative amounts Eu^{x+} as a function of the reduction time (Figure 9) are presented in Table S5.

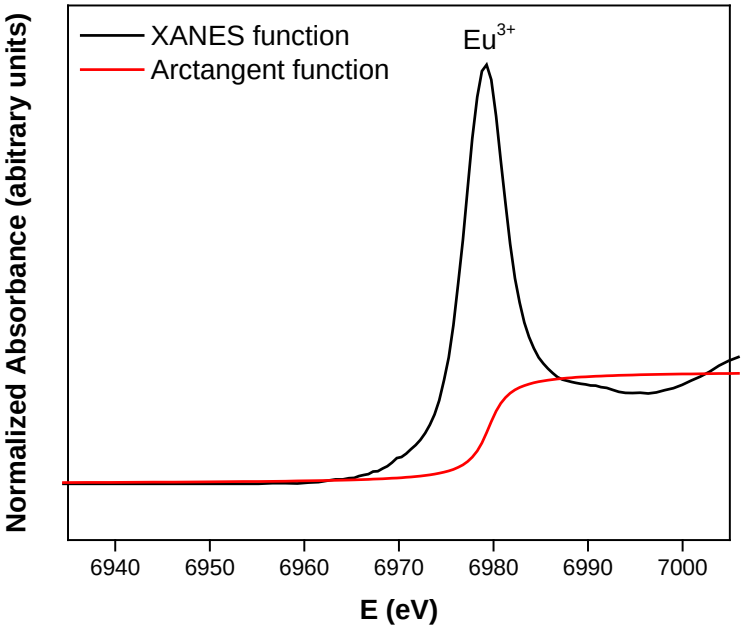

Figure S14: Arctangent background simulation (red) for a XANES spectrum after pre-edge background subtraction (black) of a solution containing 100% Eu^{3+} (66 mmol L^{-1}, 0 min of chemical reduction) in 6 mol L^{-1} $LiNO_3$.

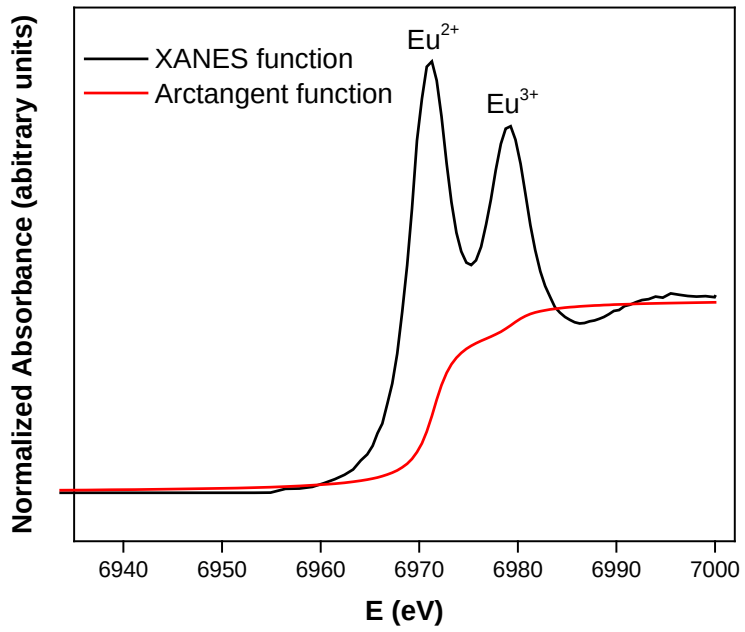

Figure S15: Arctangent background simulation (red) for a XANES spectrum after pre-edge background subtraction (black) of a solution containing both Eu^{2+} and Eu^{3+} (66 mmol L^{-1}, 90 min of chemical reduction) in 6 mol L^{-1} $LiNO_3$.

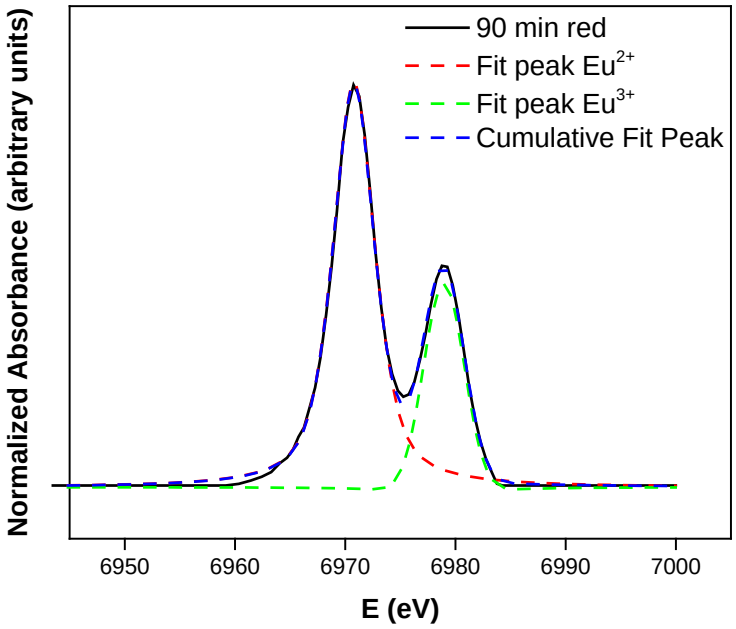

Figure S16: Peak deconvolution of a XANES spectrum (after pre-edge and arctangent background subtraction) of a solution containing both Eu^{2+} and Eu^{3+} (66 mmol L^{-1}, 90 min of chemical reduction) via multiple peak analysis by Pseudo-Voigt functions.

Table S6: Outcome of the curve parameters A, y_0 and R_0 for the function model $f(x) = y_0 + A \cdot e^{R_0 \cdot x}$ for the curve analysis of the relative amount of Eu^{x+} as a function of the reduction time.

Eu^{x+}	A	y_0	R_0
Eu^{2+}	-0.950 ± 0.045	0.984 ± 0.039	-0.0209 ± 0.00
Eu^{3+}	0.950 ± 0.045	0.016 ± 0.039	-0.0209 ± 0.00

4.2 Samples with different nitrate salt concentrations and europium content

XANES measurements on the chemical reduction of europium as a function of time were conducted on solutions containing different lithium nitrate salt concentrations (0, 3 and 6 mol L^{-1}). The results of these measurements can be found in Figure S17, Figure S18 and Figure S19, respectively. The concentration of europium in these samples was 10 times lower,

i.e. 6.6 mmol L^{-1}, resulting in poorer data quality with high background noise levels. The requirement of relatively concentrated samples is a disadvantage of the XAFS measurement techniques. Notwithstanding the poor data quality, some general trends can be distinguished. First of all, it is clear that reduction of Eu^{3+} in aqueous media containing lower nitrate salt concentration was less efficient. This might be attributed to the higher hydration of europium at these nitrate salt concentrations. Another reason might be an insufficient stabilization of Eu^{2+} in solutions containing lower nitrate salt concentrations. Secondly, 6.6 mmol L^{-1} europium remained equally well reducible in a 6 mol L^{-1} $LiNO_3$ solution compared to the samples containing 66 mmol L^{-1} europium. Thus, the reducibility of europium strongly depends on the nitrate salt concentration, with consequent change in ionic strength and activity, and seems to be independent of the europium concentration. This latter statement, however, is only valid for macro concentrations of europium in solution, as trace concentrations (10^{-10} mol L^{-1}) were impossible to test by XAFS. Peppard *et al*. already proved that stabilization of Eu^{2+} in solution at trace concentration is different compared to macro concentrations.[6,7]

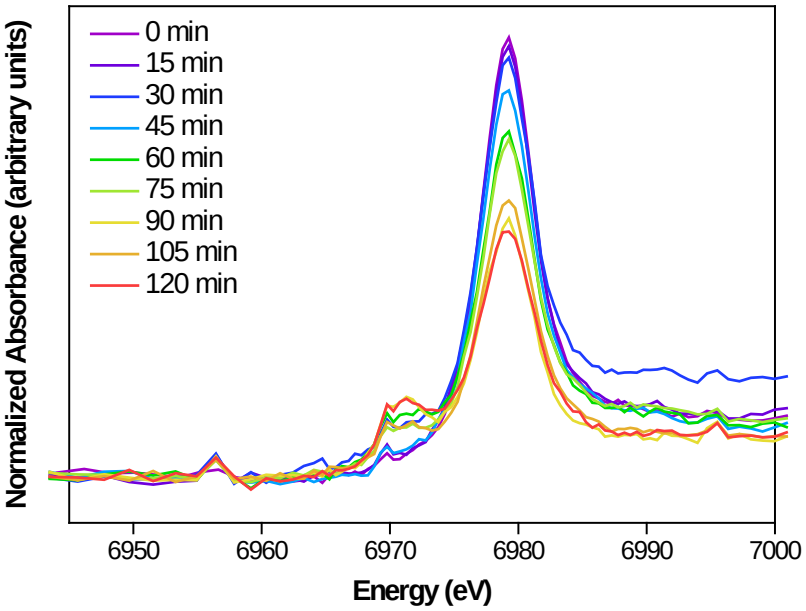

Figure S17: Normalized XANES spectra of the reduction of europium (6.6 mmol L^{-1}) in a 0 mol L^{-1} $LiNO_3$ aqueous solution as a function of time. Spectra were recorded every 15 min. The solution contained 100% Eu^{3+} at 0 min.

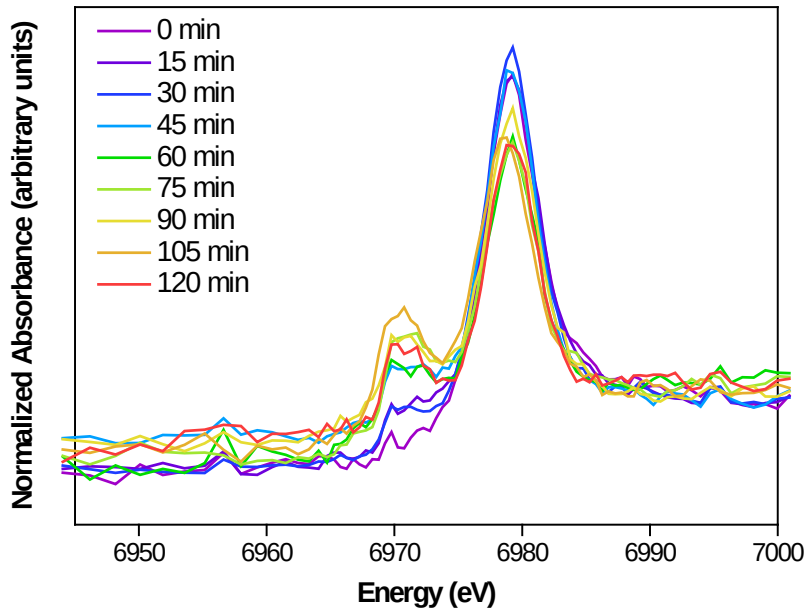

Figure S18: Normalized XANES spectra of the reduction of europium (6.6 mmol L^{-1}) in a 3 mol L^{-1} $LiNO_3$ aqueous solution as a function of time. Spectra were recorded every 15 min. The solution contained 100% Eu^{3+} at 0 min.

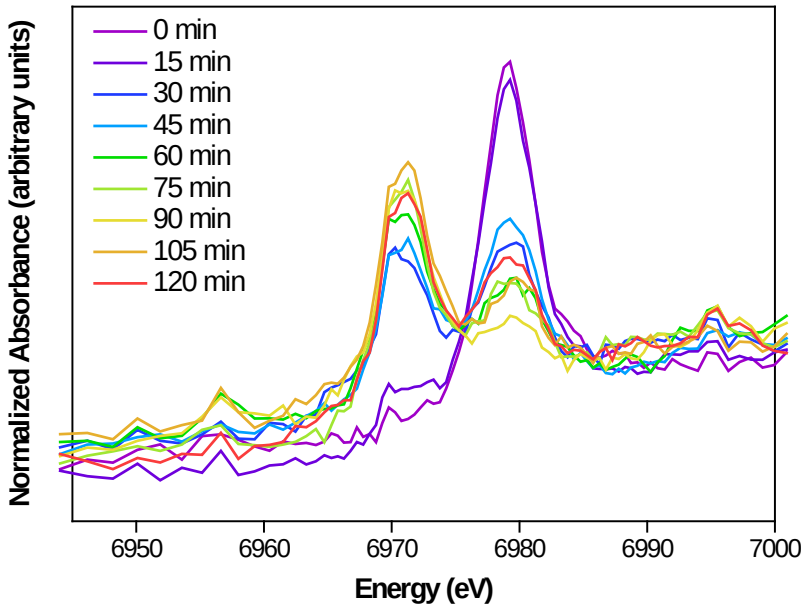

Figure S19: Normalized XANES spectra of the reduction of europium (6.6 mmol L^{-1}) in a 6 mol L^{-1} $LiNO_3$ aqueous solution as a function of time. Spectra were recorded every 15 min. The solution contained 100% Eu^{3+} at 0 min.

4.3 Stability of Eu^{2+} in nitrate aqueous solution

After chemically reducing europium (66 mmol L^{-1}) in a 6 mol L^{-1} $LiNO_3$ solution for 180 min, a XANES spectrum of a sample in a sealed measurement cell was recorded every 60 min for a period of 5 h. These XANES spectra are presented in Figure S20. These spectra were subjected to a peak analysis similar to the one described before (*vide supra*, Section 4.1) to determine the relative amounts of Eu^{2+} and Eu^{3+} in the sample. The change in relative amounts of Eu^{2+} and Eu^{3+} as a function of oxidation time after 3 h of reduction is presented in Figure S21. The parameters of the exponential fit for these curves are presented in Table S6. From these results, it is evident that Eu^{2+} is relatively stable in aqueous solutions containing a high nitrate

salt concentration when contact with air (O_2) is avoided. Only a small fraction of Eu^{2+} was found to be back-oxidized after several hours.

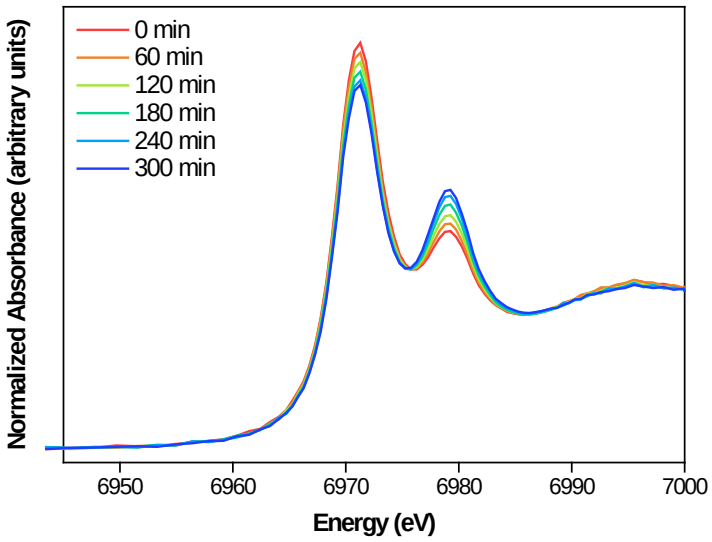

Figure S20: Normalized XANES spectra of the oxidation of europium (66 mmol L^{-1}) in a 6 mol L^{-1} $LiNO_3$ aqueous solution as a function of time after 480 min of reduction. Spectra were recorded every 60 min.

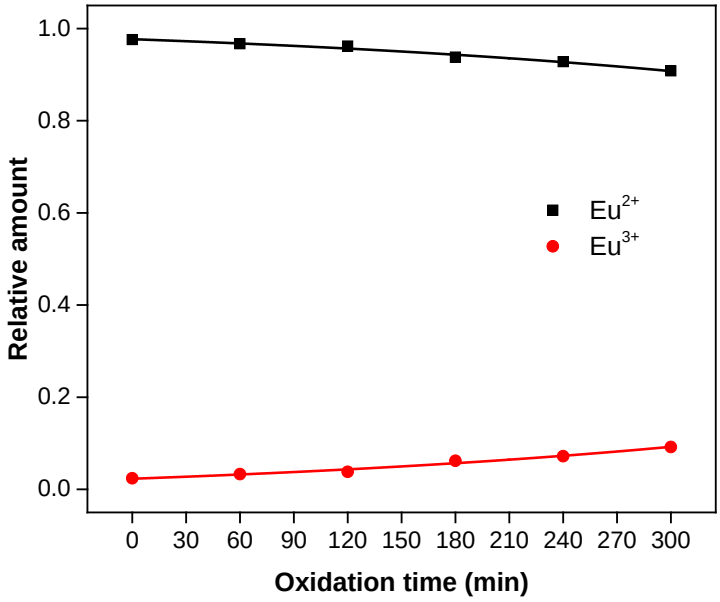

Figure S21: Indication of the relative amounts of Eu^{2+} and Eu^{3+} in a 6 mol L^{-1} $LiNO_3$ aqueous solution a function of time after europium was chemically reduced for 180 min. The XANES spectra were analyzed via Pseudo-Voigt peak deconvolution.

Table S7: Outcome of the curve parameters A, y_0 and R_0 for the function model $f(x) = y_0 + A \cdot e^{R_0 \cdot x}$ for the curve analysis of the relative amount of Eu^{x+} as a function of the oxidation time after 3 h of reduction.

Eu^{x+}	A	y_0	R_0
Eu^{2+}	-0.0451 ± 0.040	1.022 ± 0.043	0.0031 ± 0.001
Eu^{3+}	0.0451 ± 0.040	-0.022 ± 0.040	-0.0031 ± 0.001

5 References

1. K. Binnemans, *Coord. Chem. Rev.*, 2015, **295**, 1-45.
2. W. Klemm, *Systematics and the Properties of the Lanthanides*, D. Reidel Publishing Company, Dordrecht, 1983.
3. V. Kachkanov, M. J. Wallace, G. van der Laan, S. S. Dhesi, S. A. Cavill, Y. Fujiwara and K. P. O'Donnell, *Sci. Rep.*, 2012, 1-5.
4. D. A. Outka and J. Stöhr, *J. Chem. Phys.*, 1988, **88**, 3539-3554.
5. J. A. Horsley, *J. Chem. Phys.*, 1982, **76**, 1451-1458.
6. D. F. Peppard, E. P. Horwitz and G. W. Mason, *J. Inorg. Nucl. Chem.*, 1962, **24**, 429-439.
7. D.F. Peppard, E.P. Horwitz and, G. W. Mason, *US Patent,* US3077378, 1963.